crystals

Review

Binder-Free Hexagonal Boron Nitride Nanosheets (BNNSs) as Protective Coatings for Copper, Steel, and Wood: A Review

Muhammad Faheem Maqsood [1,2,†], **Syed Muhammad Zain Mehdi** [1,†], **Arslan Ashraf** [3], **Umair Azhar** [4,5], **Naseem Abbas** [6,*], **Muhammad Asim Raza** [7,*] **and Mohammed Amer** [8]

[1] Hybrid Materials Centre, Department of Nanotechnology & Advanced Materials Engineering, Sejong University, Seoul 05006, Republic of Korea
[2] Materials Science and Engineering Program, College of Arts and Sciences, American University of Sharjah, Sharjah 26666, United Arab Emirates
[3] Institute of Metallurgy & Materials Engineering, Faculty of Chemical & Materials Engineering, University of Punjab, Lahore 54590, Pakistan
[4] Department of Biology, Chemistry, and Environmental Sciences, American University of Sharjah, Sharjah 26666, United Arab Emirates
[5] Institute of Chemical and Environmental Engineering, Khwaja Fareed University of Engineering and Information Technology, Rahim Yar Khan 64200, Pakistan
[6] Department of Mechanical Engineering, Sejong University, Seoul 05006, Republic of Korea
[7] School of Chemical Engineering, Yeungnam University, Gyeongbuk 38541, Republic of Korea
[8] Department of Mechanical Engineering, Palestine Technical University—Kadoorie, Tulkarm P.O. Box 7, Palestine
* Correspondence: naseem.abbas@sejong.ac.kr (N.A.); muhammadasimraza@yu.ac.kr (M.A.R.)
† These authors contributed equally to this work.

Abstract: Hexagonal boron nitride (h-BN) has emerged as a promising dielectric material for protecting metallic substrates such as copper and steel under ambient conditions. The layered structure of h-BN offers significant potential in preventing the oxidation and corrosion of these substrates. Due to their impermeability, boron nitride nanosheets (BNNSs) do not form a galvanic cell with the underlying metals, enhancing their effectiveness as protective coatings. BNNSs are both thermally and chemically stable, making them suitable for coatings that protect against environmental degradation. Additionally, BNNSs have demonstrated excellent fire resistance, hydrophobicity, and oxidation resistance when applied to wood, functioning as a binder-free, retardant coating that remains effective up to 900 °C in air. This review focuses on the anti-corrosion properties of BNNSs, particularly on copper and steel substrates, and discusses various methods for their application. This article also discusses future perspectives in this field, including the innovative concept of wooden satellites designed for short- and long-term missions.

Keywords: boron nitride nanosheets (BNNSs); binder-free coatings; corrosion resistance; fire resistance; wooden satellite

check for updates

Academic Editor: Evgeniy N. Mokhov

Received: 19 November 2024
Revised: 1 January 2025
Accepted: 13 January 2025
Published: 20 January 2025

Citation: Maqsood, M.F.; Mehdi, S.M.Z.; Ashraf, A.; Azhar, U.; Abbas, N.; Raza, M.A.; Amer, M. Binder-Free Hexagonal Boron Nitride Nanosheets (BNNSs) as Protective Coatings for Copper, Steel, and Wood: A Review. *Crystals* **2025**, *15*, 99. https://doi.org/10.3390/cryst15010099

1. Introduction

Corrosion, the gradual chemical or electrochemical deterioration of metals, results in the loss of their integrity, strength, luster, and overall metallic properties. This phenomenon significantly impacts various industrial sectors, such as offshore extraction, natural gas extraction, and transportation, particularly when metals are exposed to corrosive agents like chloride ions, oxygen, and water [1]. While several methods, including anodic and cathodic protection, coatings, and alloying, have been developed to combat corrosion, organic polymer coatings are a relatively straightforward solution [2–9]. However, traditional coatings often suffer from defects, cracks, and shrinkage due to solvent evaporation, necessitating thicker coatings (300–500 µm) to prevent corrosion effectively [10].

To overcome this issue, various nanocomposite coatings are already prepared or in the developing stages, which exhibit superior barrier characteristics and corrosion resistance compared to a singular organic coating, attributable to the synergistic interaction between the coating matrix and nano-fillers [11,12]. For fillers, an important feature is dimensionality, like the layered two-dimensional (2D) structure, nanosheets with a thickness less than 10 nm, and lateral dimensions greater than 100 nm. These nanosheets are acknowledged for their remarkable properties in terms of specific surface area and their notable chemical, thermal, and mechanical characteristics. These characteristics render them exceptionally attractive for prospective applications in energy storage materials, catalysis, electronics, water purification, and protective coatings [13–22]. Since the discovery of graphene, extensive exploration has been conducted on a diverse array of 2D nanomaterials. This involves layered hexagonal BN (h-BN), graphitic carbon nitride, transition metal dichalcogenides, MXenes, layered double hydroxides, and others [23–31]. Due to the structural and morphological similarity of the h-BN nanosheets (BNNSs) with the graphene, it is also known as “white graphene” and received much attention due to its distinct electronic and thermodynamic characteristics. Hexagonal boron nitride (h-BN) is a white, solid material with minimal porosity, attracting significant attention for use as a protective coating due to its exceptional electronic and thermodynamic properties. Structurally, h-BN consists of boron (B) and nitrogen (N) atoms in a 1:1 ratio, arranged in stacked sp^2 hybridized honeycomb lattice structures. The material is characterized by strong B-N covalent bonds with a bond length of 1.45 Å and interlayer spacing of 0.333 nm, held together by weak van der Waals forces. The bonding between boron and nitrogen, driven by their respective electronegativities (2.04 for B and 3.04 for N), creates a slightly ionic B–N bond. This significant electronegativity difference and partial ionic character make h-BN an excellent electrical insulator with a wide band gap. Few-layered boron nitride nanosheets (BNNSs), typically ranging in thickness from 0.414 to 10 nm, possess a high aspect ratio and large surface area. These nanosheets demonstrate impressive mechanical properties, including a high bending modulus (~32 GPa) and thermal conductivity in the range of 1700 to 2000 W/m·K, making them highly effective for thermal management. Their elevated thermal and chemical stability is ascribed to robust σ-bonds, a partly ionic character, and the lack of surface states and dangling bonds, enhancing their overall durability. BNNSs also exhibit several other advantages, such as low electrical conductivity, exceptional thermal shock resistance, impermeability, non-toxic behavior, and a high dielectric constant. Their surface area (~2600 m^2/g) is significantly higher than that of BN nanotubes (212–254 m^2/g) and bulk BN (10 m^2/g), enhancing their performance in various applications. The oxidation resistance of BNNSs, which exceeds 800 °C, further positions them as ideal candidates for high-temperature, oxidation-resistant coatings [24,32,33].

Figure 1 represents the various forms of boron nitride, ranging from bulk to zero-dimensional structures, including cubic-BN (c-BN), wurtzite-BN (w-BN), hexagonal-BN (h-BN), rhombohedral-BN (r-BN), boron nitride nanotubes (BNNTs) with both single and multiwall configurations, boron nitride nanoribbons (BNNRs) featuring zigzag and armchair edges, as well as boron nitride nanocages and quantum dots [32,33]. Every nanostructure has unique physicochemical properties, such as a large specific surface area, a high band gap energy, a low dielectric constant, remarkable thermal and chemical durability, and excellent thermal conductivity. These outstanding features have led to the use of h-BN nanoparticles in diverse applications, including adsorption, photocatalytic degradation, sensor and electrical device development, medication delivery, energy storage, and more [34–36]. Properties like electrical conductivity, thermal conductivity, and applications of various types of h-BN are discussed in Table 1.

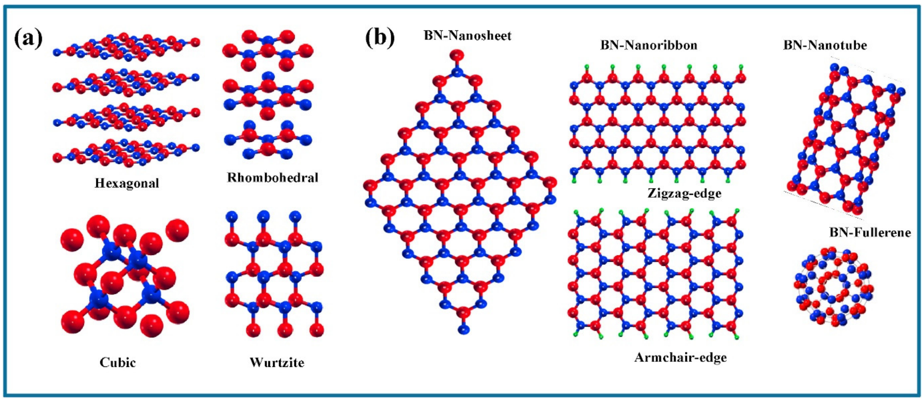

Figure 1. Structural models of boron nitride. (**a**) Bulk BN with different crystal structures like hexagonal, rhombohedral, cubic, and wurtzite, and (**b**) BN nanostructures with nanosheet, nanoribbon (zigzag and armchair configurations), nanotube, and zero-dimensional fullerene [32].

Table 1. The electrical conductivity, thermal conductivity, and typical applications of various forms of boron nitride (BN).

Types of h-BN	Type of Hybridization	Electrical Conductivity	Thermal Conductivity	Applications	Ref.
Cubic BN (c-BN)	Sp3	Insulator	~1300 W/mK	For cutting tools, insulating material in electronics, protective coatings, thermocouple protection sheaths, crucibles, protective lining for reaction vessels, ultraviolet (UV) detectors, and UV-light-emitting diodes.	[32,37–40]
Wurtzite BN (w-BN)	Sp3	Insulator	100–300 W/mK	Machining/cutting/milling ferrous and carbide materials; Optoelectronics devices; dielectric substrate material for optical, electronic, and 2D graphene-based devices; short wavelength electro-luminescent optics; and high-temperature microelectronics, transparent coatings, energy storage devices, optical sensors, thermal management systems, and durable structural components.	[32,37,41–44]
Hexagonal BN (h-BN)	Sp2	10^{-13} to 10^{-14} S/m	390–2000 W/mK	Adsorption nanomaterials, photocatalysis, membrane separation, antibiosis, environmental sensing, energy conversion and storage, and toxicity analysis.	[32,37,45–53]
Rhomohedral BN (r-BN)	Sp2	Insulator	20–300 W/mK	Cutting tools and abrasives, coating and mold release, electrical insulation, and thermal spray.	[32,37,46]
BN nanotubes (BNNTs)	Sp2	Insulator, could be a semiconductor under specific conditions	~350 W/mK	Polymer coating reinforcement, thermal management packages, piezo actuators, neutron shielding nanomaterials, self-cleaning membranes, reusable heat resistive films, biological probes, and biological channels in biosensing.	[32,37,54–61]
BN nanoribbons	Sp2	Insulator	100–400 W/mK	Adsorption, CO_2 reduction, water splitting, and environmental sensing.	[32,37,62–65]
BN quantum dots (BNQDs)	Sp2	~10^{-6} to 10^{-15} S/m	0.3–1.5 nW/K	On–off probes, bioimaging, electrochemical biosensing, photocatalytic activator, proton exchange membranes, microwave absorption material, DNA cleavage activity, and detection of cancer cells.	[32,37,66–73]

The synthesis of high-quality BNNSs is crucial for achieving optimal antioxidant and corrosion resistance. BNNSs can be produced using top-down methods (e.g., mechanical exfoliation, liquid exfoliation, and thermal expansion) and bottom-up methods (e.g., chemical vapor deposition, physical vapor deposition, laser ablation, and pulsed laser deposition) [23,24,74–76]. Several studies have explored various synthesis techniques, modifications, and applications of h-BN nanomaterials, yielding BNNSs with specific characteristics tailored for different protective applications, and some of them are mentioned in Table 2. Previous research was conducted to assess the efforts in addressing the synthesis procedures, modification efforts, and applications of h-BN nanomaterials. Like Novoselov et al., [77,78] mechanically exfoliated monolayer graphene and BNNSs. Lei et al. [79] were fortunate enough to yield up to 85% for the exfoliation process by using urea as an assistant. They developed a few layered BNNSs with 2–2.5 nm thicknesses and lateral sizes of 100 nm. Han et al. [80] demonstrated the solvent-assisted ultrasonication of single- or few-layered BNNSs by liquid phase exfoliation. Cheng et al. [81] used gas-assisted thermal expansion to develop BNNSs with 3–5 nm thicknesses, yielding up to 13.6%. Zhou et al. [82] introduced and developed BNNSs by chemical weathering with 2–4 layers of a single or bilayer structure, each layer 1 nm thick. By contrast, much research work conducted on the different applications of h-Bn, like Zheng et al. [83], noticed the varied covalent and non-covalent surface alteration methods to better the interfacial performance and dwindle the aggregation tendency of h-BN nanomaterials. Zhou et al. [84] reviewed multiple h-BN/semiconductor composite types as photocatalysts and illustrated their photocatalytic mechanism. Yu et al. [85] reviewed h-BN-based nanomaterials for the absorption of contaminants in an aqueous solution, described the removal process, and examined the effects of environmental factors on absorption.

Table 2. The various methods used for producing boron nitride nanosheets (BNNSs) and the key properties of the resulting BNNSs.

Methods Involved to Obtain BNNSs	Properties of BNNSs Obtained	Ref.
CVD	• Controllable atomic thickness • High-quality 2D single and multilayer BN thin films • Thin film with wide area homogeneity and first-class layer number selectivity • High purity and crystallinity • Relatively higher corrosion resistance and mechanical strength	[13,86–88]
Electrophoretic deposition	• Enhanced mechanical, anti-corrosion, and antitribological properties	[89–91]
Liquid phase exfoliation method	• Precise adjustments of the concentration, lateral dimension, and thickness of the generated NSs. • High-quality crystalline NSs • % yield might be low; probability of layer stacking exists.	[23,86,92]
Magnetron sputtering	• High-quality BNNSs with controlled thickness • Scalable deposition rate • High uniformity over large area • Good adhesion to substrates • Low defect density	[93–95]

This review focuses on using binder-free hexagonal boron nitride nanosheets (BNNSs) as protective coatings for copper, steel, and wood substrates. It examines the synthesis methods, structural properties, and performance of BNNS coatings in preventing corrosion, with particular attention to their application in high-temperature environments. This review also highlights recent advancements and future perspectives in developing h-BN-based protective coatings.

2. Evaluation of BNNSs Binder-Free Coating on Copper, Steel, and Wood Substrates

2.1. Evaluation of BNNSs Binder-Free Coating on Copper

Li et al. [96] conducted experiments on 20 μm thick copper (Cu) foil coated with BNNSs grown via chemical vapor deposition (CVD) using borazine as the precursor. The BNNSs formed a uniform coating on both sides of the Cu foil. The foils were oxidized in open air using a tube furnace and used for further study. Atomic force microscopy (AFM) revealed the BNNS thickness to be 7–8 nm (~20 layers) after transferring them to a silicon substrate with a 90 nm oxide layer (SiO_2/Si). Due to BN's low visible light absorption, the BN-coated Cu foil retained a metallic appearance, like bare Cu foil, as shown in Figure 2a,c and the scanning electron microscopy (SEM) surface topography in Figure 2b,d.

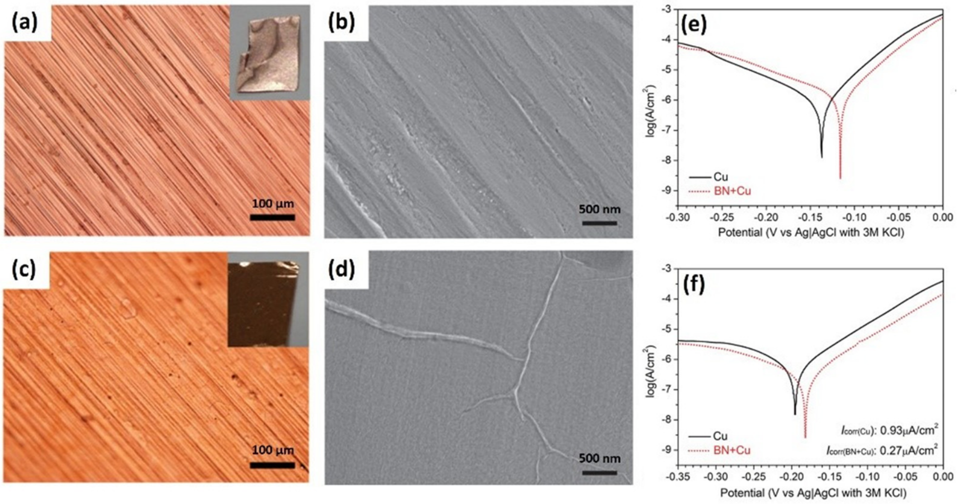

Figure 2. (**a**) Optical and (**b**) electron microscope images of bare Cu foil, (**c**) optical and (**d**) electron microscope images of BNNS-covered Cu foil, and Tafel plots of the bare and BNNS-covered Cu foil in (**e**) aerated and (**f**) nitrogen gas bubbled 0.1 M NaCl solution [96].

A Tafel analysis was used to compare the corrosion kinetics of Cu foil with and without BNNSs in an aerated NaCl solution (shown in Figure 2e,f). The BNNS-coated Cu foil had a lower anodic current but a greater cathodic current than the bare Cu sample, showing that BN nanosheets decrease Cu oxidation while increasing oxygen reduction. Cyclic voltammetry (CV) studies in a nitrogen-saturated NaCl solution verified this behavior, with the BN-coated Cu foil exhibiting lower anodic and cathodic currents and a lower corrosion current density. The corrosion current (I_{corr}) of bare Cu and BN-coated Cu was 0.93 and 0.27 $\mu A/cm^2$, respectively. The shift in corrosion potential from −0.20 V to −0.17 V for the BN-coated Cu foil implies the passivation of the underlying Cu by the BN nanosheets. A comparison of Tafel and (open circuit potential) OCP plots (shown in Figure 2) from aerated and nitrogen-saturated solutions indicated that the BN-coated Cu sample's higher cathodic and open circuit current was possibly defective due to the BN sheets. Carbon and oxygen contaminations, often found in BN crystals [97,98], along with carbon doping, can lead to the formation of boron carbide nitride, which enhances oxygen reduction [99,100]. The lower anodic current observed in the aerated solution and the significant anti-oxidation performance of the BN-coated Cu foil indicate that the oxygen reduction assisted by BN nanosheets does not enhance the production of Cu_2O on the Cu substrate.

In another study, Khan et al. [101] studied the growth of h-BN on Cu foils (0.25 mm thick, 99.98% purity). The Cu foil was pre-treated with 10% HNO_3, dried with nitrogen, and annealed at 1000 °C (solid copper) and 1100 °C (molten copper) for 40 min under a 500 sccm flow of 10% H_2/Ar gas to remove surface oxides. h-BN growth was achieved by introducing gaseous thermal breakdown products of ammonia borane for one hour at 110 °C and transported by a 100 sccm flow of 10% H_2/Ar gas. A higher flow rate (200 sccm) reduced nucleation, leading to inhomogeneous deposition. Tungsten foil was used to support molten copper due to its superior wettability. Further, they analyzed h-BN morphology, thickness, and crystallinity, varying ammonia borane quantities while maintaining the same gas mixture and substrate (Tungsten) support [102].

Post-EIS testing (after 1 h in 0.5 M NaCl), the samples' optical appearance changed noticeably. Corrosion was evident across the entire surface of the bare solid and melted Cu (Figure 3a,b), but only a few small spots appeared on the hexagonal boron nitride nanofilm (BNNF)-coated melted Cu. Further analysis using Raman spectroscopy and X-ray photoelectron spectroscopy (XPS) was conducted to examine the corrosion products after EIS tests. A Raman analysis confirmed the excellent protective performance of the high-quality BNNF on melted Cu (Figure 3c). The strong peaks at 531 and 614 cm^{-1} and shoulder peaks at 338 and 414 cm^{-1} indicated the production of $Cu(OH)_2$ or CuO on the bare Cu surface [103,104]. Weak oxidation signals were identified on solid Cu in BNNF-coated samples, but they were almost completely missing on melted Cu. In the XPS assessment (Figure 3d), the BNNF-coated melted Cu had the smallest Cl 2p peak among all samples, indicating the coat's great efficacy in preserving the surface and restricting Cl^- ion transport.

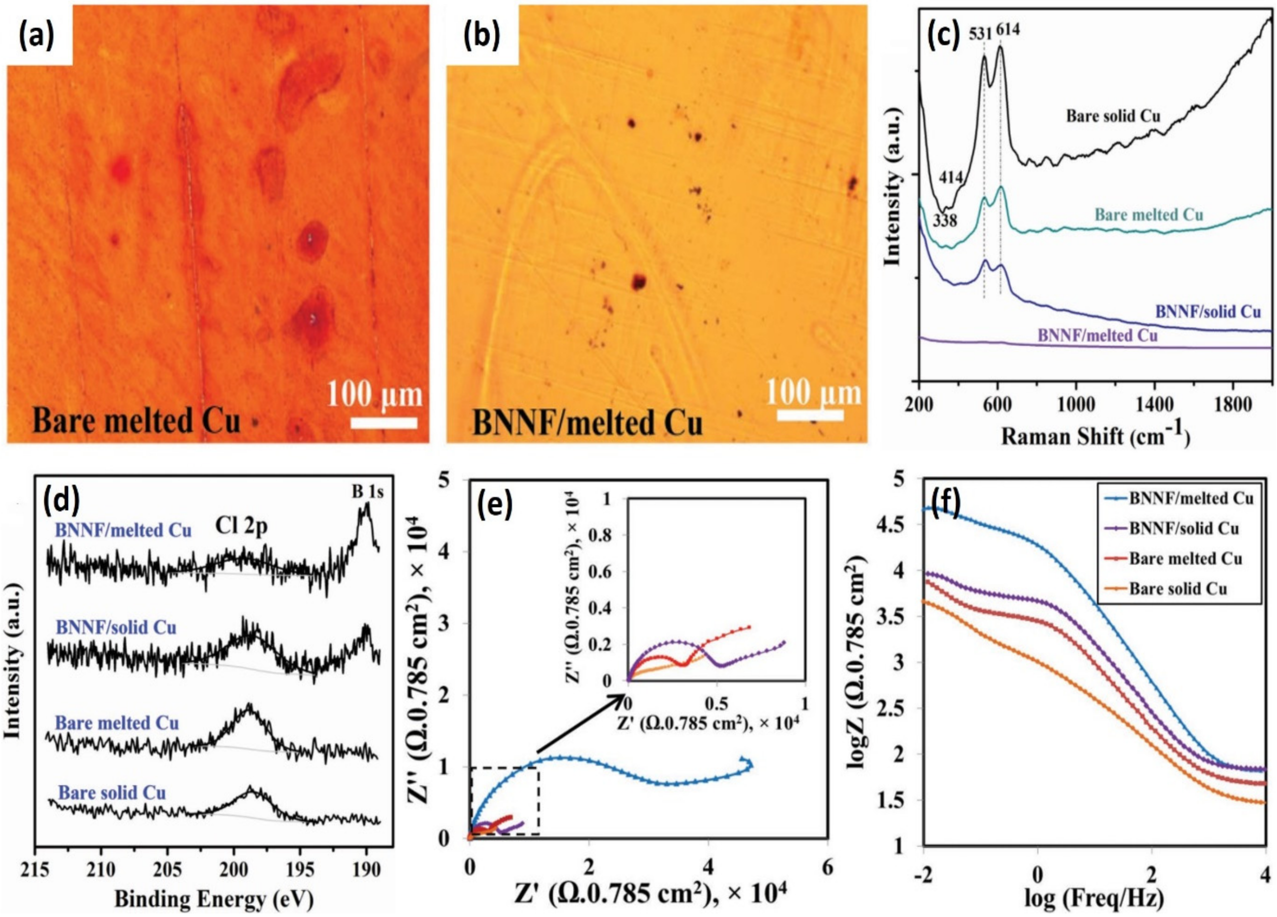

Figure 3. (**a**,**b**) Optical images of the bare and BNNF-coated Cu after the EIS tests; (**c**) Raman spectra; (**d**) XPS analysis of Cl 2p peak for the bare and BNNF-coated Cu after the EIS tests; (**e**) Nyquist plots, with the inset showing an enlargement of the high-frequency region; and (**f**) Bode plots acquired by EIS in 0.5 M NaCl solution after 5 min of immersion [101].

Electrochemical impedance spectroscopy (EIS) was conducted to evaluate the impedance properties of bare and BNNF-coated solid and melted copper (Cu). The impedance values presented in the Nyquist and Bode plots (Figure 3e,f) revealed a significant increase in impedance values for the BNNF-coated samples, highlighting the effectiveness of the coating. Among the uncoated samples, the melted Cu exhibited higher corrosion resistance than solid Cu, likely due to its larger grain size and smoother surface, which reduced the exposure of reactive Cu atoms. For the BNNF-coated melted Cu, the impedance at low frequencies was almost ten times higher than that of the bare melted Cu, underscoring the high quality of the BNNF coating. The increased low-frequency impedance linked to charge transfer in defective surface regions suggests that the hexagonal structure of BNNF effectively hinders ion diffusion, aligning with previous findings [105,106]. In a 0.5 M NaCl solution, the bare solid and melted Cu experienced a substantial rise in impedance due to the formation of thick oxides on their surfaces, whereas the BNNF-coated Cu showed significantly less increase, affirming its protective nature. Notably, the BNNF-coated melted Cu demonstrated minimal impedance change, indicating superior corrosion resistance and structural stability. After one hour of immersion, the charge transfer impedance at 0.01 Hz for the BNNF-coated melted Cu decreased slightly, likely due to surface ion absorption enhancing the charge transfer process. Importantly, the mid-frequency domain impedance of the BNNF-coated melted Cu remained unchanged, confirming its chemical stability in a saline environment.

Further, Ren et al. [107] successfully synthesized BN films on Cu foil via CVD, producing monolayer and multilayer films by adjusting deposition time. The Cu foil (25 µm thick) was pre-cleaned and annealed at 600 °C for 20 min under an Ar/H_2 gas flow, followed by heating to 1000 °C. Ammonia borane was sublimated at 120–130 °C and delivered to the reaction zone using a gas flow. The BN growth lasted 30–60 min, followed by rapid cooling. BN films were transferred using polymethyl methacrylate (PMMA) for further analysis.

The as-grown BN films were transferred onto 300 nm SiO_2/Si substrates using a PMMA-assisted method for further characterization. The thickness and uniformity of the films were evaluated using optical microscopy and AFM, as illustrated in Figure 4a–d. The green color of the films deepened as the number of layers increased. Monolayer (1 L) and multilayer BN films were tested by storing uncoated and BN-coated copper (Cu) foils under ambient conditions at room temperature for 30 days to assess oxidation resistance. After this period, the BN-coated Cu foils retained their metallic appearance, similar to uncoated Cu, owing to the atomic thickness and high optical transmittance of the BN films. At T1 (after the first 30 days), the BN-coated samples showed the same color and morphology as freshly prepared samples, indicating that even a single atomic layer of BN is an effective oxidation barrier in ambient conditions [108]. Figure 4i–l shows the surface topography of the coated foils at T1, revealing a smoother surface on the BN-coated Cu foils, further confirming their superior resistance to oxidation at room temperature. However, Cu grains and BN wrinkles became increasingly visible as the number of BN layers increased, likely due to the mismatch in thermal expansion coefficients between Cu and BN.

The XPS analysis in Figure 4o,p revealed that after 30 days of exposure, BN-coated Cu foils showed distinct metallic copper peaks at 932.6 and 952.5 eV corresponding to the Cu $2p_{3/2}$ and $2p_{1/2}$, while uncoated Cu foils exhibited broader peaks, indicating Cu_2O formation and significant oxidation [109]. These findings confirm that BN films effectively protect Cu foils from atmospheric reactions, preventing Cu oxide formation under ambient conditions. However, defects in monolayer BN films, such as wrinkles and grain boundaries, allowed localized oxidation, leading to micro-sized oxidation patches. In contrast, multilayer BN films provided better protection by hindering horizontal oxygen transport, with oxidation occurring mainly at wrinkles where oxygen reached the Cu surface through meandering pathways.

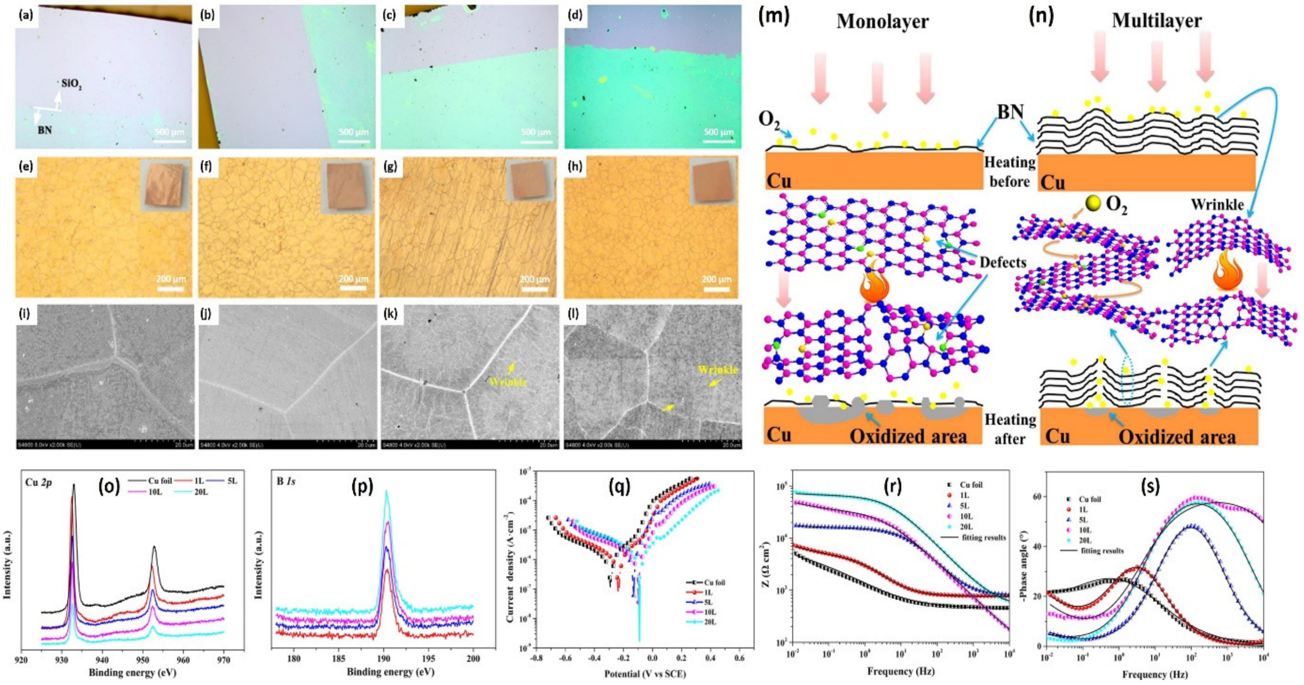

Figure 4. Optical images of (**a**) 1 L, (**b**) 5 L, (**c**) 10 L, and (**d**) 20 L BN films; digital camera photos of BN-coated Cu foil after 30 days exposure at room temperature (**e**) 1 L, (**f**) 5 L, (**g**) 10 L, and (**h**) 20 L; SEM images of BN-coated Cu foil after 30 days exposure at room temperature (**i**) 1 L, (**j**) 5 L, (**k**) 10 L, and (**l**) 20 L; schematic diagrams of the oxidation mechanisms for the (**m**) monolayer and (**n**) multilayer BN films; (**o**,**p**) XPS spectra of BN-coated and uncoated Cu foils after 30 days exposure at room temperature; (**q**) potentiodynamic polarization plots; (**r**) Bode plots; and (**s**) phase angle vs. frequency plots of the BN-coated and uncoated Cu foils [107].

The corrosion resistance of BN-coated and uncoated Cu foils was assessed through electrochemical measurements in a 3.5 wt.% NaCl solution. The potentiodynamic polarization test results in Figure 4q show that the BN-coated Cu foils displayed higher corrosion potentials (E_{corr}) and significantly lower anodic current densities (I_{corr}) than uncoated Cu foils. The E_{corr} and I_{corr} values for uncoated Cu foils were -0.29 V and 9.23×10^{-5} A/cm^2, respectively, while those for BN-coated Cu foils ranged from -0.24 V and 1.12×10^{-6} A/cm^2 (1 L) to -0.088 V and 4.62×10^{-7} A/cm^2 (20 L). The 20 L BN-coated Cu foil demonstrated a positive E_{corr} shift of 0.202 V and a remarkable 200-fold reduction in I_{corr} compared to the uncoated sample. The Bode plots in Figure 4r revealed that the impedance modulus values at the lowest frequency (Zf = 0.01 Hz) of BN-coated Cu foils ranged from 1.3 times (1 L) to 14 times (20 L) higher than those of uncoated foils, with a notable improvement in Zf = 0.01 Hz as the number of BN layers increased from 1 L to 10 L. However, the rate of impedance increase diminished beyond 10 layers. These results highlight that even a few atomic layers of BN provide substantial corrosion protection for Cu foils, significantly mitigating their susceptibility to degradation in saline environments.

While in another study, A. Nadeem and M.A. Raza [91] successfully deposited BNNSs on copper using electrophoretic deposition (EPD). They prepared BNNSs by dispersing 125 mg of h-BN powder in 125 mL isopropyl alcohol (IPA), sonicated for 35 h, centrifuged at 4000 rpm, and used the supernatant for deposition. A Cu strip and platinum electrode served as the cathode and anode, respectively, with 50 μL of HCl added to enhance conductivity before deposition. The X-ray diffraction (XRD) pattern of both the h-BN powder and the BNNS-coated Cu sample (deposited for 5 min) is presented in Figure 5a.

The BNNS-coated Cu sample shows a distinct peak at 2θ = 26.78°, corresponding to the typical (002) peak of BNNSs, confirming the successful deposition of BNNSs on the Cu substrate by EPD. The additional peaks in the BNNS-coated Cu sample are attributed to the underlying Cu planes. Figure 5 also displays photographs of the bare Cu sample, the BNNS-coated sample at 90 V for 1 min, and the BNNS-coated sample at 90 V for 5 min.

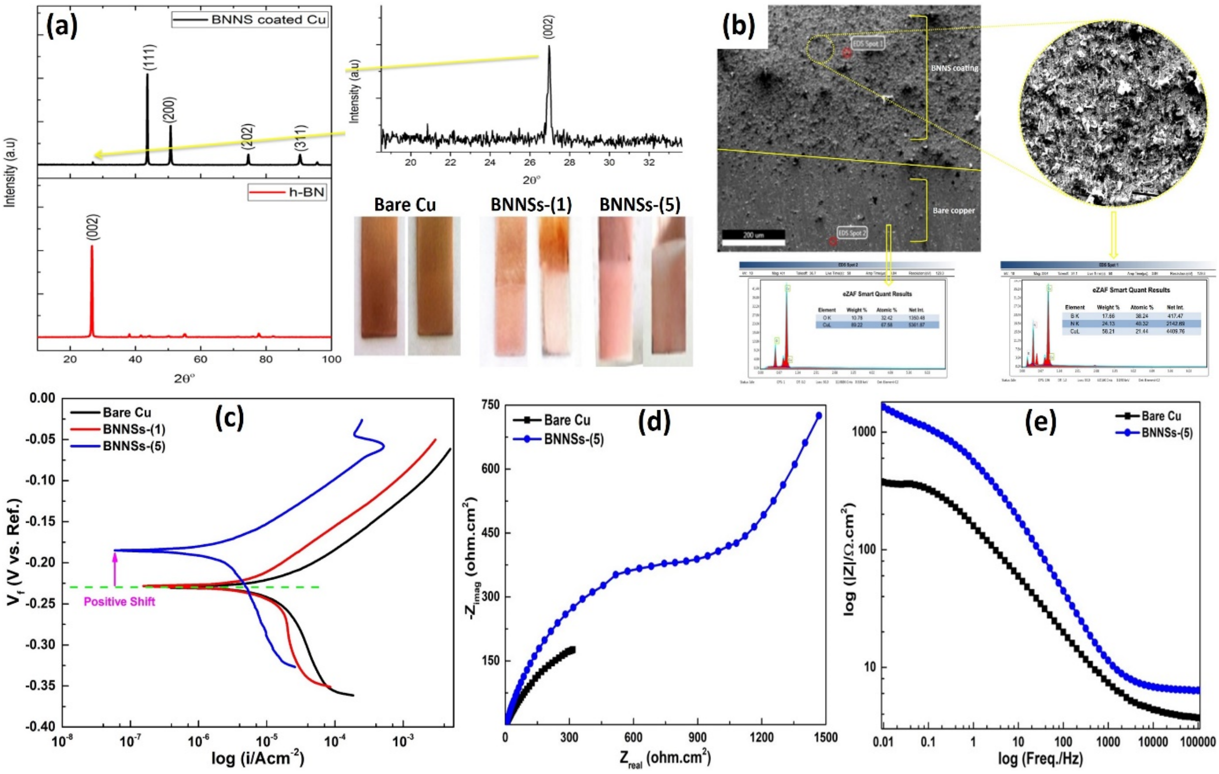

Figure 5. (**a**) XRD pattern of h-BN (commercial) and BNNSs-(5), (**b**) SEM and EDX spectrums of bare Cu and with BNNSs-(5), (**c**) Tafel plotting of bare Cu and BNNSs coated samples, and (**d**) Nyquist and (**e**) Bode curves of BNNSs-(5) vs. bare Cu samples [91].

The SEM and energy-dispersive X-ray spectroscopy (EDX) analysis of commercial h-BN and BNNSs developed by sonication are shown in Figure 5b. A SEM analysis reveals that h-BN consists of large particles, whereas BNNSs are smaller, flat sheets with slightly smaller lateral dimensions than h-BN. Both h-BN and BNNSs contain boron (B) and nitrogen (N) elements, as confirmed by the EDX analysis. The Cu sample's coated portion shows uniform BNNS coverage with a slightly rough topography, consistent with AFM observations.

Tafel plots were generated to evaluate the corrosion resistance of uncoated Cu and BNNS-coated Cu samples deposited via EPD. The BNNS-coated samples, prepared at 90 V for 1 min (BNNS-(1)) and 5 min (BNNS-(5)), demonstrated a positive shift in corrosion potential (E_{corr}). For BNNS-(5), E_{corr} shifted to −185 mV compared to −230 mV for bare Cu, indicating improved corrosion resistance. Furthermore, the corrosion current density (I_{corr}) of BNNS-(5) decreased significantly to 4.80 $\mu A/cm^2$ from 21.40 $\mu A/cm^2$ for bare Cu, reflecting a nearly sixfold reduction in the corrosion rate. The Tafel analysis also revealed that BNNS-(5) offered better corrosion resistance than BNNS-(1). EIS was performed to investigate the corrosion mechanisms further. Nyquist and Bode plots showed that BNNS-(5) exhibited higher impedance across both high and low frequencies than bare Cu, confirming its superior corrosion protection. These results underscore the enhanced protective performance of the BNNS coating, particularly for BNNS-(5), in reducing corrosion susceptibility.

2.2. Evaluation of BNNSs Binder-Free Coating on Steel

A. Nadeem et al. [110] successfully deposited BNNSs on mild steel (MS) using CVD. Pre-treated 1 × 2 cm^2 MS strips were etched with 5% HCl, sonicated, and cleaned with 1 M NaOH. In the CVD process, 100 mg of boron powder and the MS samples were placed in a quartz tube, evacuated to 1 bar, and exposed to ammonia gas at 200–250 sccm. The furnace was heated to 1200 °C at 50 °C/min and held for 30–180 min before cooling overnight in the sealed tube. Figure 6a presents SEM images of the BNNS-coated MS substrate, clearly showing the deposition of BNNSs. The coating predominantly consists of BNNSs (approximately 80%), with some ribbons and boron nitride nanotubes (BNNTs) also forming. This occurrence is likely due to the iron in the mild steel acting as a catalyst for BNNT growth [111]. Additionally, some pores are visible in the image. The FTIR spectra of BNNS-coated MS samples, subjected to deposition at 1200 °C for varying durations, are shown in Figure 6b, reveal two strong transmission peaks at 1330 cm^{-1} and 760 cm^{-1}, corresponding to sp^2-bonded B-N and B-N-B bending vibrations, respectively [112]. These characteristic peaks in all BNNS-coated samples confirm the successful deposition of BNNSs across all temperatures. The Raman spectra of commercial BN and BNNS-coated MS are displayed in Figure 6c, further corroborating these findings. The BNNS-coated MS samples exhibit two characteristic peaks at 1377.69 cm^{-1} (commercial BN) and 1366.49 cm^{-1} (BNNSs), corresponding to the E2g vibration mode of BN [113]. The slight shift in the B-N bond peak in the BNNS-coated MS compared to the commercial BN (1366–1377 cm^{-1}) suggests that the BN was deposited as turbostratic nanosheets [114].

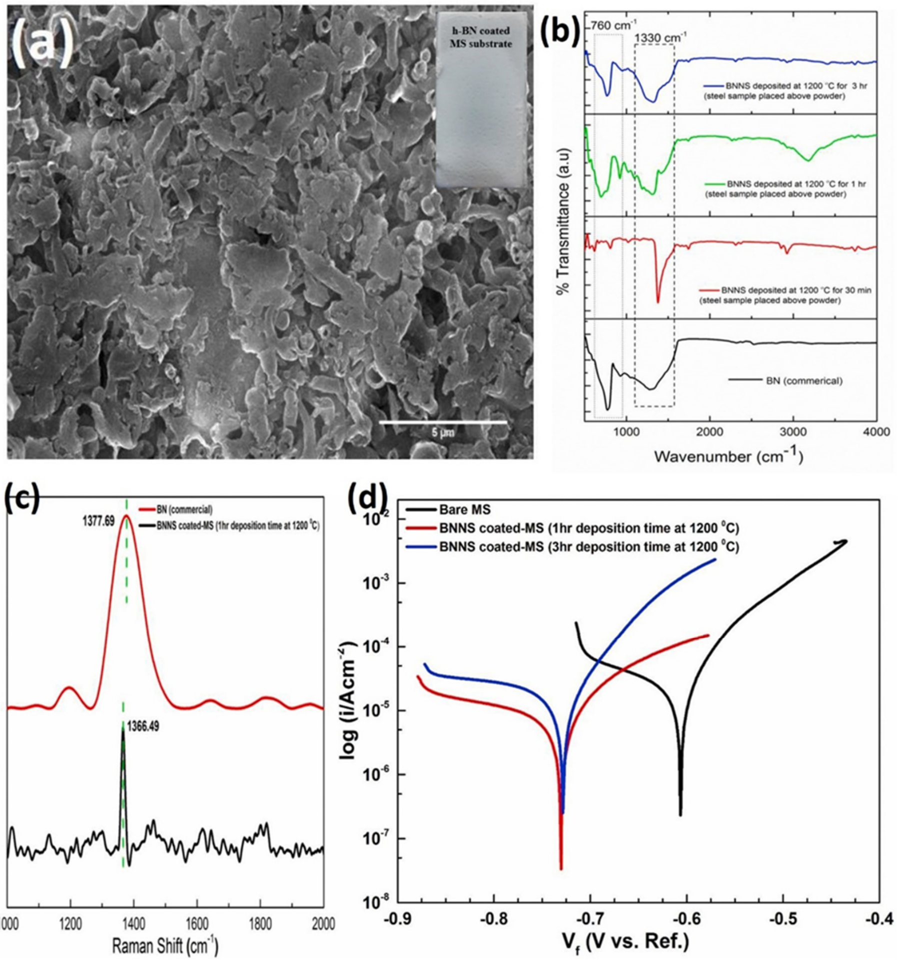

Figure 6. (**a**) SEM of BNNS-coated MS with inset digital camera photo (1 h deposition time at 1200 °C), (**b**) FTIR curves, (**c**) Raman spectra, and (**d**) Tafel curves of BNNS-coated MS sample [110].

A Tafel analysis of bare MS and BNNS-coated MS samples, produced at 1200 °C for 1 h and 3 h, is shown in Figure 6d. The BNNS-coated samples exhibited a shift in corrosion potential (E_{corr}) toward more negative values and a significant reduction in corrosion current density (I_{corr}) compared to the bare MS. This decrease in I_{corr} indicates that the BNNS coating effectively inhibits ion oxidation and enhances oxygen reduction [115]. The presence of carbon and oxygen impurities in the BN crystal and potential carbon doping from the MS at high deposition temperatures (1200 °C) likely leads to the formation of boron carbonitride, further facilitating oxygen reduction. The observed negative shift in E_{corr} suggests that BNNSs act as a cathodic coating, providing electrical insulation and minimizing the risk of galvanic corrosion. Specifically, the I_{corr} of the BNNS-coated MS sample, deposited for 1 h at 1200 °C, decreased from 32.0 $\mu A/cm^2$ (bare MS) to 15.9 $\mu A/cm^2$, demonstrating a twofold improvement in corrosion resistance [116].

Meanwhile, Tang et al. [117] explored the deposition of h-BN films directly onto SS304 stainless steel substrates using RF magnetron sputtering. The 10×10 mm^2 substrates were polished and pre-cleaned through ultrasonic treatments in diluted HCl, alcohol, and deionized water. During deposition, the chamber pressure was maintained below 1×10^{-5} Pa, and a sintered BN target, mounted on a water-cooled magnetron gun, was powered at 90–150 W. The substrates, positioned 8 cm from the target, were heated to 650 °C and biased with a pulsed voltage. Nitrogen and Ar gases flowed at 50 sccm, and the working pressure was set to 2 Pa. The BN target was pre-sputtered for 3 min to ensure cleanliness before the 3 h deposition process, successfully forming h-BN films on the stainless steel.

The SEM images illustrating the direct growth of h-BN nanofilms on the ss304 substrate are shown in Figure 7a–c. Figure 7a presents the SEM images of the bare ss304, while Figure 7b shows the h-BN-coated substrate. The images confirm that the h-BN films are continuous over a large area, closely following the morphology of the pristine substrate surface. The uncoated ss304 surface appears shiny and bright, but after applying the h-BN coating, the surface takes on a yellowish hue. The visible scratches on the SS304 surface reveal the partial transparency of the h-BN film. The consistent coloration across the coated substrate indicates that the h-BN film is uniform and continuous. As shown in Figure 7c, the h-BN coating fully covers the SS304 surface, filling cracks and grain boundaries inherent to the substrate. This comprehensive coverage provides robust protection against oxidation and corrosion, enhancing the durability of the SS304 surface.

Figure 7d presents the XRD patterns of the SS304 substrate before and after h-BN deposition. The uncoated SS304 substrate exhibits characteristic diffraction peaks at $2\theta = 43.8°$, 50.9°, and 75.1°, corresponding to the (100), (200), and (220) planes of austenitic stainless steel [118]. Following h-BN growth, an additional weak (002) diffraction peak at 26.7° is observed, indicating that the h-BN film predominantly consists of nanocrystalline domains with a preferential (002) plane orientation on the SS304 substrate. An FTIR analysis, performed in reflection mode due to the non-transparency of SS304 in the IR region, is shown in Figure 7e. The spectrum reveals two prominent peaks at 820 cm^{-1} and 1549 cm^{-1}, corresponding to transverse optical (TO) B-N-B out-of-plane bending vibrations [119] and longitudinal optical (LO) in-plane B-N stretching vibrations of sp^2-bonded h-BN, respectively. A weak shoulder at 1380 cm^{-1} is also observed, attributed to TO in-plane B-N vibrations. These findings confirm the presence of pure h-BN in the film without any detectable impurities. At the same time, the TO-LO splitting suggests an ordered texture within the deposited h-BN film [120]. Figure 7f displays the Raman spectrum of the SS304 substrate after h-BN deposition, highlighting a pronounced E2g peak at 1367 cm^{-1}, characteristic of h-BN [119]. The full width at half maximum (FWHM) of the h-BN/SS304 film is measured at 27 cm^{-1}, significantly narrower than the FWHM of the few-layer h-BN directly grown on other substrates (60 cm^{-1}) [121], though slightly wider than the h-BN atomic layers grown on Cu foils (14.5 cm^{-1}) [122] and transferred h-BN on SiO_2/Si (23 cm^{-1}) [121]. These results suggest that the h-BN coating is of high quality and offers effective corrosion protection for metallic surfaces.

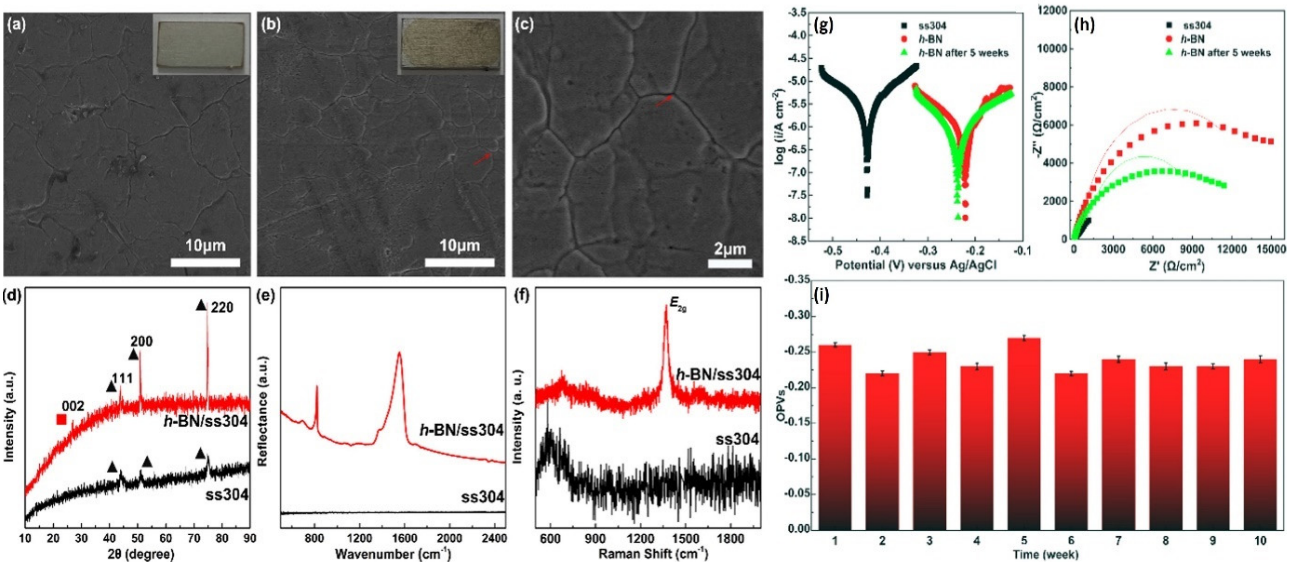

Figure 7. SEM images of (**a**) bare ss304 and (**b**,**c**) h-BN/ss304 with inset digital camera photo (h-BN coated at 650 °C with 150 rf power and 0 V bias), (**d**) XRD, (**e**) FTIR and (**f**) Raman spectra of ss304 and h-BN/ss304 for comparison, (**g**) Tafel curves and (**h**) Nyquist plots of samples immersed in 3.5% NaCl for five weeks, and (**i**) OCP stability of h-BN/ss304 for a total of 10 weeks [117].

Figure 7g,h illustrate the Tafel curve and Nyquist plot for the h-BN-coated SS304 sample after five weeks of immersion in a 3.5% NaCl solution. The Tafel curve shows no significant changes in E_{corr} or I_{corr} over the five weeks, suggesting that the h-BN coating effectively maintains its protective properties. While the Nyquist plot indicates a decrease in impedance resistance, as evidenced by a reduction in the semicircle diameter, the impedance values remain comparable in magnitude to those of the freshly coated film. Figure 7i shows the open circuit potential (OCP) analysis of the h-BN-coated ss304 substrate, where the OCP voltage (OPV) remained relatively stable, with only minor fluctuations. This indicates the durability and consistency of the h-BN coating in providing corrosion protection over time.

2.3. Evaluation of BNNSs Binder-Free Coating on Wood

Liu et al. [123] developed BN nanosheets via liquid-phase exfoliation and applied them as coatings on cedar wood. Bulk BN powder (4 g) was dispersed in a 1 mg/mL sodium dodecyl benzenesulfonate (SDBS) solution and sonicated for 4 h with heat regulation. After resting overnight, the mixture was centrifuged to isolate a semi-transparent BN nanosheet suspension, further concentrated by high-speed centrifugation. For comparison, BN was also exfoliated in IPA under similar steps. The final BN nanosheet coatings adhered strongly to the cedar wood substrate, filling grooves and creating a uniform layer, forming a 1–5 μm thick layer, demonstrating their durability and protective potential.

The elemental composition of the exfoliated h-BN nanosheets was characterized using Raman spectroscopy. The Raman spectra, shown in Figure 8a, feature a distinct peak at 1365.8 cm^{-1}, corresponding to the E2g vibrational mode of h-BN [124]. The FWHM of this peak is approximately 5.21 cm^{-1} for the exfoliated BN nanosheets, which is slightly broader than that of bulk BN powder (4.77 cm^{-1}) [125]. This minor increase in the FWHM suggests the high quality of the exfoliated nanosheets despite the reduction in interlayer interactions caused by the exfoliation process. Additionally, the variation in the intensity of the E2g mode reflects changes in the material's structural dynamics due to the exfoliation [126].

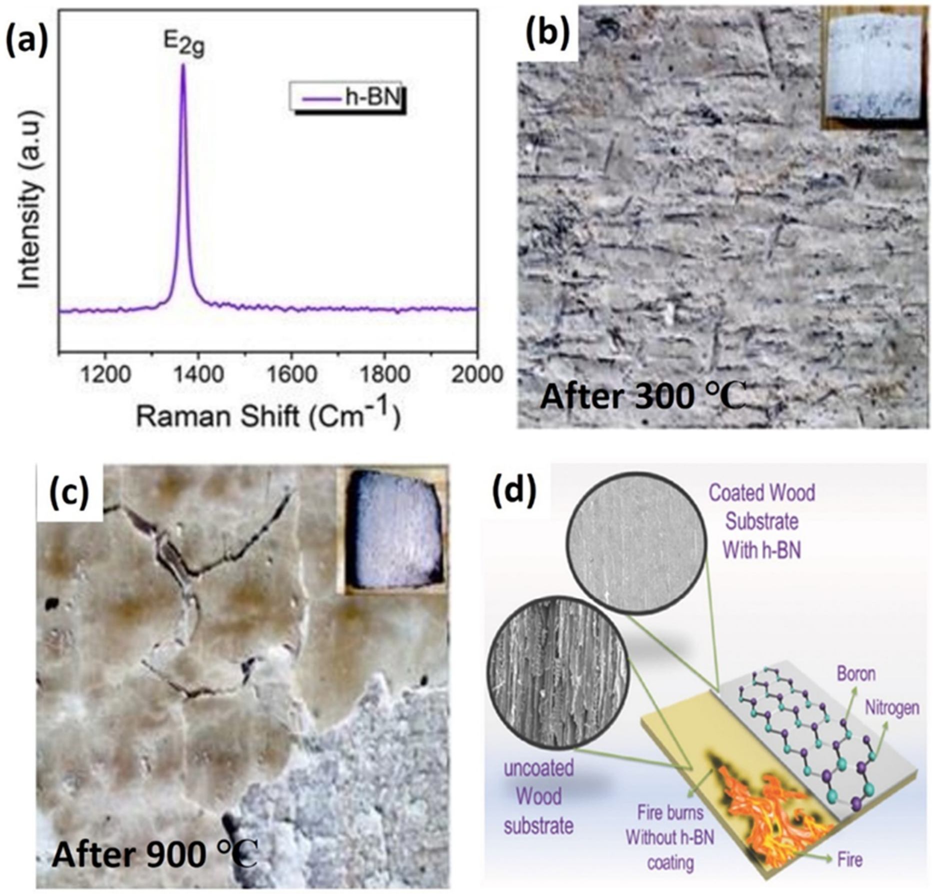

Figure 8. (**a**) Raman spectra of BNNS-coated wood substrate, oxidation resistance property of BNNS-coated wood substrate at (**b**) 300 °C and (**c**) 900 °C, and (**d**) schematic illustration of the experiment [123].

Oxidation resistance experiments were conducted at 300 °C and 900 °C by exposing the h-BN-coated substrates to these temperatures. As shown in Figure 8b, no visible damage occurred to the coating at 300 °C. However, at 900 °C, significant morphological changes were observed (Figure 8c). The h-BN coating began to deteriorate and separate from the wood substrate, likely due to the thermal expansion of the wood at high temperatures. The darkening of the coating indicates its degradation, though the underlying wood remained largely unaffected by oxidation. Despite the coating's withering, no significant mass loss was observed up to 900 °C, suggesting that the h-BN nanosheet coating, with an optimal thickness, enhances the oxidation resistance of wood products under high temperatures and oxygen-rich environments. Figure 8d provides a schematic illustration of the oxidation resistance experiments.

3. Conclusions and Future Perspectives

This review emphasizes the application of binder-free hexagonal boron nitride nanosheets (BNNSs) as protective coatings for copper, steel, and wood substrates. The absence of organic binders is a key advantage, as it allows the inherent properties of h-BN—such as its exceptional mechanical strength, high thermal stability, hydrophobicity, and chemical inertness—to be fully realized without interference. These characteristics make BNNS coatings highly suitable for environments prone to corrosion, oxidation, and wear. However, achieving the desired performance depends significantly on the quality of the nanosheets and their direct adhesion to the substrate, which is particularly critical in binder-free systems. The ability of h-BN to form a protective boron oxide layer when exposed to oxygen further enhances corrosion resistance. At the same time, its anisotropic thermal properties are particularly effective for insulating wood substrates by minimizing thermal diffusivity and effusivity.

Despite these promising attributes, several challenges limit the widespread use of binder-free BNNS coatings, primarily related to the uniform dispersion and strong adhesion of BNNSs on various substrates. The flake-like structure of BNNSs poses a challenge due to its tendency to aggregate, which compromises its ability to form continuous, defect-free coatings. Future research should focus on advanced surface modification techniques to improve the compatibility and alignment of BNNSs on diverse substrates. Structural modifications, such as functionalization with specific chemical groups, could significantly enhance adhesion and, consequently, these coatings' durability and protective performance. Additionally, exploring hybrid structures combining BNNSs with other two-dimensional materials like graphene offers a promising route for enhancing the mechanical and protective properties while retaining the advantages of a binder-free system.

From the structural design perspective, further research should emphasize the development of multilayer BNNS coatings, which can enhance barrier properties against environmental degradation and mechanical wear. The ordered arrangement of BNNS layers could improve resistance to ion diffusion and moisture penetration, making these coatings more effective in preventing corrosion. Traditional corrosion characterization methods should be supplemented with advanced computational techniques, such as quantum chemistry and molecular dynamics simulations, to fully understand the protective mechanisms and optimize these coatings. These methods will provide valuable insights into the molecular-level interactions between BNNS coatings and corrosive agents, allowing for more targeted design improvements.

Current challenges in the field also include achieving consistent and uniform layer deposition (binder-free or with binder) across various substrates (Al, Mg, Cu, Fe, Ni, etc.) without sacrificing the nanosheets' intrinsic properties. Future efforts should aim to refine exfoliation and deposition processes to produce monodispersed BNNSs with controlled thickness and lateral dimensions. This will be key to preventing agglomeration, a significant factor that currently diminishes the protective capabilities of BNNS coatings. Additionally, optimizing these processes could enable the application of BNNS coatings in more industrially relevant settings, including high-temperature and high-humidity environments.

The long-term stability and durability of binder-free BNNS coatings under diverse environmental conditions must be a priority before they can be widely adopted in the industry. In aerospace and satellite applications, these coatings offer tremendous potential for providing lightweight yet durable protection against extreme conditions such as radiation, high temperatures, and oxidative environments. The absence of organic binders ensures that these coatings maintain their structural integrity over time, making them ideal for prolonged exposure in space. Future research should explore the role of BNNS coatings in improving thermal management, resistance to space weathering, and overall durability under the harsh conditions of outer space as proposed in Figure 9. Such innovations could lead to the development of advanced materials for aerospace applications, contributing to the reduction in space debris by eliminating the need for conventional metallic paints that degrade over time. By addressing these challenges through innovative structural design and process optimization, BNNS coatings can be better positioned as a robust solution for corrosion protection in a variety of industrial and high-performance applications.

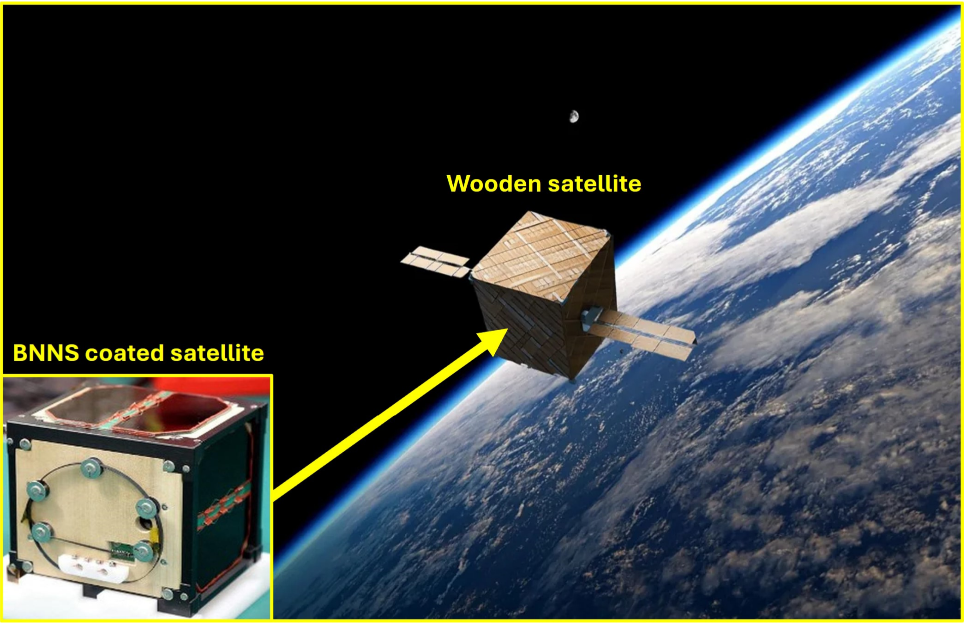

Figure 9. Prospective application of binder-free BNNS coatings for wooden satellite.

Author Contributions: Conceptualization, writing—original draft preparation, and investigation, M.F.M. and S.M.Z.M.; methodology, A.A.; formal analysis, U.A. and M.A.; data curation, writing—review and editing, and supervision, N.A.; funding acquisition, N.A. and M.A.R. All authors have read and agreed to the published version of the manuscript.

Funding: This research received no external funding.

Data Availability Statement: No new data were created or analyzed in this study.

Acknowledgments: The authors thank the American University of Sharjah and Sejong University for their support. The Basic Science Research Program supported this research through the National Research Foundation of Korea (NRF) funded by the Ministry of Education (NRF-2020R1A6A1A03043435 and NRF- 2021R1A2C1008798). Additionally, we extend our appreciation to ChatGPT for its assistance and insights during the preparation of this article [127].

Conflicts of Interest: Authors declare no conflicts of interest.

References

1. Zhao, H.; Yue, Y.; Guo, L.; Wu, J.; Zhang, Y.; Li, X.; Mao, S.; Han, X. Cloning Nacre's 3D Interlocking Skeleton in Engineering Composites to Achieve Exceptional Mechanical Properties. *Adv. Mater.* **2016**, *28*, 5099–5105. [CrossRef]
2. Verma, C.; Ebenso, E.E.; Quraishi, M.A. Corrosion inhibitors for ferrous and non-ferrous metals and alloys in ionic sodium chloride solutions: A review. *J. Mol. Liq.* **2017**, *248*, 927–942. [CrossRef]
3. Ormellese, M.; Beretta, S.; Brugnetti, F.; Brenna, A. Effects of non-stationary stray current on carbon steel buried pipelines under cathodic protection. *Constr. Build. Mater.* **2021**, *281*, 122645. [CrossRef]
4. Osipenko, M.A.; Kharitonov, D.S.; Makarova, I.V.; Romanovsky, V.I.; Kurilo, I.I. Corrosion Behavior of Modified Anodic Oxide Coatings on AD31 Aluminium Alloy. *Prot. Met. Phys. Chem. Surf.* **2021**, *57*, 550–558. [CrossRef]
5. Yanagimoto, H.; Saito, K.; Takahashi, H.; Chiba, M. Changes in the structure and corrosion protection ability of porous anodic oxide films on pure Al and Al alloys by pore sealing treatment. *Materials* **2022**, *15*, 8544. [CrossRef]
6. Nadeem, A.; Maqsood, M.F.; Raza, M.A.; Karim, M.R.; Ghafoor, F.; Lee, Y.; Ali, S.; Rehman, M.A.; Khan, M.F. Thermally stable and anti-corrosive polydimethyl siloxane composite coatings based on nanoforms of boron nitride. *Inorg. Chem. Commun.* **2024**, *168*, 112989. [CrossRef]
7. Maqsood, M.F.; Raza, M.A.; Ghauri, F.A.; Rehman, Z.U.; Ilyas, M.T. Corrosion study of graphene oxide coatings on AZ31B magnesium alloy. *J. Coat. Technol. Res.* **2020**, *17*, 1321–1329. [CrossRef]
8. Maqsood, M.F.; Raza, M.A.; Rehman, Z.U.; Abid, M.; Inam, A.; Iqbal, S. Corrosion study of zinc rich epoxy ester paints for cold galvanizing of mild steel. *Surf. Rev. Lett.* **2021**, *28*, 2150064. [CrossRef]

9. Maqsood, M.F.; Raza, M.A.; Rehman, Z.U.; Tayyeb, A.; Makhdoom, M.A.; Ghafoor, F.; Latif, U.; Khan, M.F. Role of Solvent Used in Development of Graphene Oxide Coating on AZ31B Magnesium Alloy: Corrosion Behavior and Biocompatibility Analysis. *Nanomaterials* **2022**, *12*, 3745. [CrossRef]
10. Huang, H.; Sheng, X.; Tian, Y.; Zhang, L.; Chen, Y.; Zhang, X. Two-dimensional nanomaterials for anticorrosive polymeric coatings: A review. *Ind. Eng. Chem. Res.* **2020**, *59*, 15424–15446. [CrossRef]
11. Habibiyan, A.; Ramezanzadeh, B.; Mahdavian, M.; Bahlakeh, G.; Kasaeian, M. Rational assembly of mussel-inspired polydopamine (PDA)-Zn (II) complex nanospheres on graphene oxide framework tailored for robust self-healing anti-corrosion coatings application. *Chem. Eng. J.* **2020**, *391*, 123630. [CrossRef]
12. Xia, Z.; Liu, G.; Dong, Y.; Zhang, Y. Anticorrosive epoxy coatings based on polydopamine modified molybdenum disulfide. *Prog. Org. Coat.* **2019**, *133*, 154–160. [CrossRef]
13. Khan, M.H.; Liu, H.K.; Sun, X.; Yamauchi, Y.; Bando, Y.; Golberg, D.; Huang, Z. Few-atomic-layered hexagonal boron nitride: CVD growth, characterization, and applications. *Mater. Today* **2017**, *20*, 611–628. [CrossRef]
14. Li, M.; Huang, G.; Chen, X.; Yin, J.; Zhang, P.; Yao, Y.; Shen, J.; Wu, Y.; Huang, J. Perspectives on environmental applications of hexagonal boron nitride nanomaterials. *Nano Today* **2022**, *44*, 101486. [CrossRef]
15. Abubakr, M.; Elahi, E.; Rehman, S.; Dahshan, A.; Khan, M.A.; Rabeel, M.; Abbas, Z.; Maqsood, M.F.; Rehman, M.A.; Jonghwa, E. Innovations in self-powered nano-photonics of emerging and flexible two-dimensional materials. *Mater. Today Phys.* **2023**, *39*, 101285. [CrossRef]
16. Kanwal, R.; Maqsood, M.F.; Raza, M.A.; Inam, A.; Waris, M.; Rehman, Z.U.; Mehdi, S.M.Z.; Abbas, N.; Lee, N. Polypyrrole coated carbon fiber/magnetite/graphene oxide reinforced hybrid epoxy composites for high strength and electromagnetic interference shielding. *Mater. Today Commun.* **2024**, *38*, 107684. [CrossRef]
17. Latif, U.; Raza, M.A.; Rehman, Z.U.; Iqbal, J.; Lee, N.; Mehdi, S.M.Z.; Maqsood, M.F.; Hussain, S. Binder free heteroatom-doped graphene oxide as high energy density electrodes for supercapacitor applications. *Int. J. Energy Res.* **2022**, *46*, 9643–9666. [CrossRef]
18. Latif, U.; Raza, M.A.; Rehman, Z.U.; Maqsood, M.F.; Mehdi, S.M.Z.; Ali, S.; Khan, M.F.; Kumar, S. Role of sulfur and phosphorous doping on the electrochemical performance of graphene oxide-based electrodes. *Electrochim. Acta* **2024**, *497*, 144581. [CrossRef]
19. Maqsood, M.F.; Zubair, M.A.A.; Raza, M.A.; Mehdi, S.M.Z.; Lee, N.; Rehman, Z.U.; Park, K.; Bhatti, M.U.; Latif, U.; Tawakkal, A. Fabrication and characterization of graphene oxide and glass fiber-based hybrid epoxy composites. *Polym. Compos.* **2022**, *43*, 8072–8083. [CrossRef]
20. Raza, M.A.; Rehman, Z.U.; Tanvir, M.G.; Maqsood, M.F. Metal oxide-conducting polymer-based composite electrodes for energy storage applications. In *Renewable Polymers and Polymer-Metal Oxide Composites*; Elsevier: Amsterdam, The Netherlands, 2022; pp. 195–251.
21. Rehman, Z.U.; Raza, M.A.; Chishti, U.N.; Hussnain, A.; Maqsood, M.F.; Iqbal, M.Z.; Iqbal, M.J.; Latif, U. Role of Carbon Nanomaterials on Enhancing the Supercapacitive Performance of Manganese Oxide-Based Composite Electrodes. *Arab. J. Sci. Eng.* **2022**, *48*, 8371–8386. [CrossRef]
22. Raza, M.A.; Maqsood, M.F.; Rehman, Z.U.; Westwood, A.; Inam, A.; Sattar, M.M.S.; Ghauri, F.A.; Ilyas, M.T. Thermally Reduced Graphene Oxide-Reinforced Acrylonitrile Butadiene Styrene Composites Developed by Combined Solution and Melt Mixing Method. *Arab. J. Sci. Eng.* **2020**, *45*, 9559–9568. [CrossRef]
23. Saji, V.S. 2D hexagonal boron nitride (h-BN) nanosheets in protective coatings: A literature review. *Heliyon* **2023**, *9*, e19362. [CrossRef]
24. Nadeem, A.; Raza, M.A.; Maqsood, M.F.; Ilyas, M.T.; Westwood, A.; Rehman, Z.U. Characterization of boron nitride nanosheets synthesized by boron-ammonia reaction. *Ceram. Int.* **2020**, *46*, 20415–20422. [CrossRef]
25. Ghafoor, F.; Kim, H.; Ghafoor, B.; Rehman, S.; Khan, M.A.; Aziz, J.; Rabeel, M.; Maqsood, M.F.; Dastgeer, G.; Lee, M.-J. Interface engineering in ZnO/CdO hybrid nanocomposites to enhanced resistive switching memory for neuromorphic computing. *J. Colloid Interface Sci.* **2024**, *659*, 1–10. [CrossRef]
26. Latif, U.; Maqsood, M.F. Lanthanum-zinc mixed metal oxide as electrode material for supercapacitor applications. *Mater. Chem. Phys.* **2024**, *317*, 129158. [CrossRef]
27. Latif, U.; Rehman, Z.U.; Maqsood, M.F.; Raza, M.A.; Ali, S.; Iqbal, M.J.; Mehdi, S.M.Z.; Lee, N. In situ growth of nickel ammonium phosphate ribbons on nickel foam for supercapacitor applications. *J. Energy Storage* **2023**, *73*, 109024. [CrossRef]
28. Maqsood, M.F.; Latif, U.; Sheikh, Z.A.; Abubakr, M.; Rehman, S.; Khan, K.; Khan, M.A.; Kim, H.; Ouladsmane, M.; Rehman, M.A. A comprehensive study of Bi2Sr2Co2Oy misfit layered oxide as a supercapacitor electrode material. *Inorg. Chem. Commun.* **2023**, *158*, 111487. [CrossRef]
29. Maqsood, M.F.; Latif, U.; Mehdi, S.M.Z.; Rehman, Z.U.; Raza, M.A.; Ghafoor, F.; Abubakr, M.; Lee, N.; Khan, M.F. Effect of “Mn” substitution at B-site, on the crystal structure and energy storage performance of the $La_{0.75}Sr_{0.25}CoO_3$ perovskite. *J. Ind. Eng. Chem.* **2024**, *39*, 587–600. [CrossRef]

30. Rehman, Z.U.; Raza, M.A.; Tariq, A.; Chishti, U.N.; Maqsood, M.F.; Lee, N.; Awais, M.H.; Mehdi, S.M.Z.; Inam, A. $La_{0.75}Sr_{0.25}Cr_{0.5}Mn_{0.5}O_3$ perovskite developed for supercapacitor applications. *J. Energy Storage* **2020**, *32*, 101951. [CrossRef]
31. Huang, Y.; Zhao, C.; Li, Y.; Wang, C.; Yuan, W.; Shen, T.; Liu, J.; Cheng, D.; Wu, C.; Shen, Q. A smart sol-gel coating incorporating pH-responsive BTA-ZIF-8 MOF assembled hexagonal boron nitride for active/passive corrosion protection of 1060 aluminum alloy. *Surf. Coat. Technol.* **2023**, *474*, 130072. [CrossRef]
32. Sharma, V.; Kagdada, H.L.; Jha, P.K.; Śpiewak, P.; Kurzydłowski, K.J. Thermal transport properties of boron nitride based materials: A review. *Renew. Sustain. Energy Rev.* **2020**, *120*, 109622. [CrossRef]
33. Arenal, R.; Lopez-Bezanilla, A. Boron nitride materials: An overview from 0D to 3D (nano)structures. *WIREs Comput. Mol. Sci.* **2015**, *5*, 299–309. [CrossRef]
34. Shtansky, D.V.; Matveev, A.T.; Permyakova, E.S.; Leybo, D.V.; Konopatsky, A.S.; Sorokin, P.B. Recent Progress in Fabrication and Application of BN Nanostructures and BN-Based Nanohybrids. *Nanomaterials* **2022**, *12*, 2810. [CrossRef] [PubMed]
35. Tay, R.Y.; Li, H.; Wang, H.; Lin, J.; Ng, Z.K.; Shivakumar, R.; Bolker, A.; Shakerzadeh, M.; Tsang, S.H.; Teo, E.H.T. Advanced nano boron nitride architectures: Synthesis, properties and emerging applications. *Nano Today* **2023**, *53*, 102011. [CrossRef]
36. Shtansky, D.V.; Firestein, K.L.; Golberg, D.V. Fabrication and application of BN nanoparticles, nanosheets and their nanohybrids. *Nanoscale* **2018**, *10*, 17477–17493. [CrossRef]
37. Angizi, S.; Alem, S.A.A.; Azar, M.H.; Shayeganfar, F.; Manning, M.I.; Hatamie, A.; Pakdel, A.; Simchi, A. A comprehensive review on planar boron nitride nanomaterials: From 2D nanosheets towards 0D quantum dots. *Prog. Mater. Sci.* **2022**, *124*, 100884. [CrossRef]
38. Rathinasabapathy, S.; Santhosh, M.; Asokan, M. Significance of boron nitride in composites and its applications. In *Recent Advances in Boron-Containing Materials*; IntechOpen: London, UK, 2020; p. 63.
39. Ronning, C.; Feldermann, H.; Hofsäss, H. Growth, doping and applications of cubic boron nitride thin films. *Diam. Relat. Mater.* **2000**, *9*, 1767–1773. [CrossRef]
40. Mohammad, S.N. Electrical characteristics of thin film cubic boron nitride. *Solid-State Electron.* **2002**, *46*, 203–222. [CrossRef]
41. Fedoseev, D.; Lavrent'ev, A.; Varshavskaya, I.; Bochko, A.; Karyuk, G. Determination of the thermal conductivities of refractory materials with the aid of an optical quantum generator. *Sov. Powder Metall. Met. Ceram.* **1978**, *17*, 240–241. [CrossRef]
42. Liu, Y.; Zhan, G.; Wang, Q.; He, D.; Zhang, J.; Liang, A.; Moellendick, T.E.; Zhao, L.; Li, X. Hardness of Polycrystalline Wurtzite boron nitride (wBN) compacts. *Sci. Rep.* **2019**, *9*, 10215. [CrossRef]
43. Chkhartishvili, L. Density of electron states in wurtzite-like boron nitride: A quasi-classical calculation. *Mater. Sci. Ind. J.* **2006**, *2*, 18–23.
44. Hayat, A.; Sohail, M.; Hamdy, M.S.; Taha, T.; AlSalem, H.S.; Alenad, A.M.; Amin, M.A.; Shah, R.; Palamanit, A.; Khan, J. Fabrication, characteristics, and applications of boron nitride and their composite nanomaterials. *Surf. Interfaces* **2022**, *29*, 101725. [CrossRef]
45. Chen, C.-C.; Li, Z.; Shi, L.; Cronin, S.B. Thermoelectric transport across graphene/hexagonal boron nitride/graphene heterostructures. *Nano Res.* **2015**, *8*, 666–672. [CrossRef]
46. McKinney, R.; Gorai, P.; Toberer, E.S.; Stevanovic, V. Rapid prediction of anisotropic lattice thermal conductivity: Application to layered materials. *Chem. Mater.* **2019**, *31*, 2048–2057. [CrossRef]
47. Maiti, K.; Thanh, T.D.; Sharma, K.; Hui, D.; Kim, N.H.; Lee, J.H. Highly efficient adsorbent based on novel cotton flower-like porous boron nitride for organic pollutant removal. *Compos. Part B Eng.* **2017**, *123*, 45–54. [CrossRef]
48. Duan, L.; Wang, B.; Heck, K.; Guo, S.; Clark, C.A.; Arredondo, J.; Wang, M.; Senftle, T.P.; Westerhoff, P.; Wen, X. Efficient photocatalytic PFOA degradation over boron nitride. *Environ. Sci. Technol. Lett.* **2020**, *7*, 613–619. [CrossRef]
49. Hafeez, A.; Karim, Z.A.; Ismail, A.F.; Samavati, A.; Said, K.A.M.; Selambakkannu, S. Functionalized boron nitride composite ultrafiltration membrane for dye removal from aqueous solution. *J. Membr. Sci.* **2020**, *612*, 118473. [CrossRef]
50. Kaviya, S.; Kabila, S.; Jayasree, K. Hexagonal bottom-neck ZnO nano pencils: A study of structural, optical and antibacterial activity. *Mater. Lett.* **2017**, *204*, 57–60. [CrossRef]
51. Bian, Y.; Li, L.; Song, H.; Su, Y.; Lv, Y. Porous boron nitride: A novel metal-free cataluminescence material for high performance H2S sensing. *Sens. Actuators B Chem.* **2021**, *332*, 129512. [CrossRef]
52. Babamiri, O.; Vanaei, A.; Guo, X.; Wu, P.; Richter, A.; Ng, K. Numerical Simulation of Water Quality and Self-Purification in a Mountainous River Using QUAL2KW. *J. Environ. Inform.* **2021**, *37*, 26–35. [CrossRef]
53. Mateti, S.; Wong, C.S.; Liu, Z.; Yang, W.; Li, Y.; Li, L.H.; Chen, Y. Biocompatibility of boron nitride nanosheets. *Nano Res.* **2018**, *11*, 334–342. [CrossRef]
54. Zhi, C.; Bando, Y.; Terao, T.; Tang, C.; Kuwahara, H.; Golberg, D. Towards Thermoconductive, Electrically Insulating Polymeric Composites with Boron Nitride Nanotubes as Fillers. *Adv. Funct. Mater.* **2009**, *19*, 1857–1862. [CrossRef]
55. Zeng, X.; Sun, J.; Yao, Y.; Sun, R.; Xu, J.-B.; Wong, C.-P. A combination of boron nitride nanotubes and cellulose nanofibers for the preparation of a nanocomposite with high thermal conductivity. *ACS Nano* **2017**, *11*, 5167–5178. [CrossRef]

56. Nakhmanson, S.M.; Calzolari, A.; Meunier, V.; Bernholc, J.; Nardelli, M.B. Spontaneous polarization and piezoelectricity in boron nitride nanotubes. *Phys. Rev. B* **2003**, *67*, 235406. [CrossRef]
57. Kang, J.H.; Sauti, G.; Park, C.; Yamakov, V.I.; Wise, K.E.; Lowther, S.E.; Fay, C.C.; Thibeault, S.A.; Bryant, R.G. Multifunctional electroactive nanocomposites based on piezoelectric boron nitride nanotubes. *ACS Nano* **2015**, *9*, 11942–11950. [CrossRef]
58. Li, L.H.; Chen, Y. Superhydrophobic properties of nonaligned boron nitride nanotube films. *Langmuir* **2010**, *26*, 5135–5140. [CrossRef]
59. Lim, H.; Suh, B.L.; Kim, M.J.; Yun, H.; Kim, J.; Kim, B.J.; Jang, S.G. High-performance, recyclable ultrafiltration membranes from P4VP-assisted dispersion of flame-resistive boron nitride nanotubes. *J. Membr. Sci.* **2018**, *551*, 172–179. [CrossRef]
60. Chen, X.; Wu, P.; Rousseas, M.; Okawa, D.; Gartner, Z.; Zettl, A.; Bertozzi, C.R. Boron nitride nanotubes are noncytotoxic and can be functionalized for interaction with proteins and cells. *J. Am. Chem. Soc.* **2009**, *131*, 890–891. [CrossRef]
61. Hilder, T.A.; Gordon, D.; Chung, S.H. Boron nitride nanotubes selectively permeable to cations or anions. *Small* **2009**, *5*, 2870–2875. [CrossRef]
62. Liu, T.; Li, Y.-L.; He, J.-Y.; Hu, Y.; Wang, C.-M.; Zhang, K.-S.; Huang, X.-J.; Kong, L.-T.; Liu, J.-H. Porous boron nitride nanoribbons with large width as superior adsorbents for rapid removal of cadmium and copper ions from water. *New J. Chem.* **2019**, *43*, 3280–3290. [CrossRef]
63. Tang, S.; Zhou, X.; Zhang, S.; Li, X.; Yang, T.; Hu, W.; Jiang, J.; Luo, Y. Metal-free boron nitride nanoribbon catalysts for electrochemical CO_2 reduction: Combining high activity and selectivity. *ACS Appl. Mater. Interfaces* **2018**, *11*, 906–915. [CrossRef]
64. Fan, G.; Wang, Q.; Liu, X.; Li, C.; Xu, H. Computational screening of bifunctional single atom electrocatalyst based on boron nitride nanoribbon for water splitting. *Appl. Catal. A Gen.* **2021**, *622*, 118235. [CrossRef]
65. Srivastava, P.; Sharma, V.; Jaiswal, N.K. Adsorption of COCl2 gas molecule on armchair boron nitride nanoribbons for nano sensor applications. *Microelectron. Eng.* **2015**, *146*, 62–67. [CrossRef]
66. Yao, Q.; Feng, Y.; Rong, M.; He, S.; Chen, X. Determination of nickel (II) via quenching of the fluorescence of boron nitride quantum dots. *Microchim. Acta* **2017**, *184*, 4217–4223. [CrossRef]
67. Xue, Q.; Zhang, H.; Zhu, M.; Wang, Z.; Pei, Z.; Huang, Y.; Huang, Y.; Song, X.; Zeng, H.; Zhi, C. Hydrothermal synthesis of blue-fluorescent monolayer BN and BCNO quantum dots for bio-imaging probes. *RSC Adv.* **2016**, *6*, 79090–79094. [CrossRef]
68. Yola, M.L.; Atar, N. Development of cardiac troponin-I biosensor based on boron nitride quantum dots including molecularly imprinted polymer. *Biosens. Bioelectron.* **2019**, *126*, 418–424. [CrossRef]
69. Yang, Y.; Zhang, C.; Huang, D.; Zeng, G.; Huang, J.; Lai, C.; Zhou, C.; Wang, W.; Guo, H.; Xue, W. Boron nitride quantum dots decorated ultrathin porous g-C3N4: Intensified exciton dissociation and charge transfer for promoting visible-light-driven molecular oxygen activation. *Appl. Catal. B Environ.* **2019**, *245*, 87–99. [CrossRef]
70. Lei, Z.; Xu, S.; Wan, J.; Wu, P. Facile preparation and multifunctional applications of boron nitride quantum dots. *Nanoscale* **2015**, *7*, 18902–18907. [CrossRef]
71. Fan, L.; Zhou, Y.; He, M.; Tong, Y.; Zhong, X.; Fang, J.; Bu, X. Facile microwave approach to controllable boron nitride quantum dots. *J. Mater. Sci.* **2017**, *52*, 13522–13532. [CrossRef]
72. Umrao, S.; Maurya, A.; Shukla, V.; Grigoriev, A.; Ahuja, R.; Vinayak, M.; Srivastava, R.; Saxena, P.; Oh, I.-K.; Srivastava, A. Anticarcinogenic activity of blue fluorescent hexagonal boron nitride quantum dots: As an effective enhancer for DNA cleavage activity of anticancer drug doxorubicin. *Mater. Today Bio* **2019**, *1*, 100001. [CrossRef]
73. Radhakrishnan, S.; Park, J.H.; Neupane, R.; de los Reyes, C.A.; Sudeep, P.M.; Paulose, M.; Martí, A.A.; Tiwary, C.S.; Khabashesku, V.N.; Varghese, O.K. Fluorinated boron nitride quantum dots: A new 0D material for energy conversion and detection of cellular metabolism. *Part. Part. Syst. Charact.* **2019**, *36*, 1800346. [CrossRef]
74. Yu, R.; Yuan, X. Rising of boron nitride: A review on boron nitride nanosheets enhanced anti-corrosion coatings. *Prog. Org. Coat.* **2024**, *186*, 107990. [CrossRef]
75. Zhao, S.; Zhou, F.; Li, Z.; Liu, H. Effect of precursor purity and flow rate on the CVD growth of hexagonal boron nitride. *J. Alloys Compd.* **2016**, *688*, 1006–1012. [CrossRef]
76. Verma, C.; Dubey, S.; Barsoum, I.; Alfantazi, A.; Ebenso, E.E.; Quraishi, M. Hexagonal boron nitride as a cutting-edge 2D material for additive application in anticorrosive coatings: Recent progress, challenges and opportunities. *Mater. Today Commun.* **2023**, *35*, 106367. [CrossRef]
77. Novoselov, K.S.; Geim, A.K.; Morozov, S.V.; Jiang, D.-e.; Zhang, Y.; Dubonos, S.V.; Grigorieva, I.V.; Firsov, A.A. Electric field effect in atomically thin carbon films. *Science* **2004**, *306*, 666–669. [CrossRef]
78. Novoselov, K.S.; Jiang, D.; Schedin, F.; Booth, T.; Khotkevich, V.; Morozov, S.; Geim, A.K. Two-dimensional atomic crystals. *Proc. Natl. Acad. Sci. USA* **2005**, *102*, 10451–10453. [CrossRef]
79. Lei, W.; Mochalin, V.N.; Liu, D.; Qin, S.; Gogotsi, Y.; Chen, Y. Boron nitride colloidal solutions, ultralight aerogels and freestanding membranes through one-step exfoliation and functionalization. *Nat. Commun.* **2015**, *6*, 8849. [CrossRef]
80. Han, W.-Q.; Wu, L.; Zhu, Y.; Watanabe, K.; Taniguchi, T. Structure of chemically derived mono-and few-atomic-layer boron nitride sheets. *Appl. Phys. Lett.* **2008**, *93*, 223103. [CrossRef]

81. Cheng, Z.-l.; Ma, Z.-s.; Ding, H.-l.; Liu, Z. Environmentally friendly, scalable exfoliation for few-layered hexagonal boron nitride nanosheets (BNNSs) by multi-time thermal expansion based on released gases. *J. Mater. Chem. C* **2019**, *7*, 14701–14708. [CrossRef]
82. Zhao, G.; Zhang, F.; Wu, Y.; Hao, X.; Wang, Z.; Xu, X. One-step exfoliation and hydroxylation of boron nitride nanosheets with enhanced optical limiting performance. *Adv. Opt. Mater.* **2016**, *4*, 141–146. [CrossRef]
83. Zheng, Z.; Cox, M.; Li, B. Surface modification of hexagonal boron nitride nanomaterials: A review. *J. Mater. Sci.* **2018**, *53*, 66–99. [CrossRef]
84. Zhou, C.; Lai, C.; Zhang, C.; Zeng, G.; Huang, D.; Cheng, M.; Hu, L.; Xiong, W.; Chen, M.; Wang, J. Semiconductor/boron nitride composites: Synthesis, properties, and photocatalysis applications. *Appl. Catal. B Environ.* **2018**, *238*, 6–18. [CrossRef]
85. Yu, S.; Wang, X.; Pang, H.; Zhang, R.; Song, W.; Fu, D.; Hayat, T.; Wang, X. Boron nitride-based materials for the removal of pollutants from aqueous solutions: A review. *Chem. Eng. J.* **2018**, *333*, 343–360. [CrossRef]
86. Zhang, Y.; Sun, J.; Xiao, X.; Wang, N.; Meng, G.; Gu, L. Graphene-like two-dimensional nanosheets-based anticorrosive coatings: A review. *J. Mater. Sci. Technol.* **2022**, *129*, 139–162. [CrossRef]
87. Sun, J.; Lu, C.; Song, Y.; Ji, Q.; Song, X.; Li, Q.; Zhang, Y.; Zhang, L.; Kong, J.; Liu, Z. Recent progress in the tailored growth of two-dimensional hexagonal boron nitride via chemical vapour deposition. *Chem. Soc. Rev.* **2018**, *47*, 4242–4257. [CrossRef] [PubMed]
88. Liu, Z.; Gong, Y.; Zhou, W.; Ma, L.; Yu, J.; Idrobo, J.C.; Jung, J.; MacDonald, A.H.; Vajtai, R.; Lou, J. Ultrathin high-temperature oxidation-resistant coatings of hexagonal boron nitride. *Nat. Commun.* **2013**, *4*, 2541. [CrossRef] [PubMed]
89. Saji, V.S. Electrophoretic (EPD) coatings for magnesium alloys. *J. Ind. Eng. Chem.* **2021**, *103*, 358–372. [CrossRef]
90. Raza, M.A.; Nadeem, A.; Ilyas, M.T. Corrosion Study of Boron Nitride Nanosheets Deposited on Copper Metal by Electrophoretic Deposition. In *TMS 2019 148th Annual Meeting & Exhibition Supplemental Proceedings*; Springer: Cham, Switzerland, 2019.
91. Nadeem, A.; Raza, M. Corrosion Study of Boron Nitride Nanosheets Deposited on Copper Metal by Electrophoretic Deposition. *J. Pak. Inst. Chem. Eng.* **2021**, *49*, 85–93.
92. Gonzalez Ortiz, D.; Pochat-Bohatier, C.; Cambedouzou, J.; Bechelany, M.; Miele, P. Exfoliation of hexagonal boron nitride (h-BN) in liquide phase by ion intercalation. *Nanomaterials* **2018**, *8*, 716. [CrossRef]
93. Liu, M.; Yang, Y.; Mao, Q.; Wei, Y.; Li, Y.; Ma, N.; Liu, H.; Liu, X.; Huang, Z. Influence of radio frequency magnetron sputtering parameters on the structure and performance of SiC films. *Ceram. Int.* **2021**, *47*, 24098–24105. [CrossRef]
94. Wu, Y.; Liu, J.; Cao, H.; Wu, Z.; Wang, Q.; Ma, Y.; Jiang, H.; Wen, F.; Pei, Y. On the adhesion and wear resistance of DLC films deposited on nitrile butadiene rubber: A Ti-C interlayer. *Diam. Relat. Mater.* **2020**, *101*, 107563. [CrossRef]
95. Li, Q.; Zhang, Q.; Chen, R.; Zhang, H.; Wang, M.; Zhu, J.; Wang, X.; Liu, Y.; Yun, F. Wafer− Scale Growth of Fe− Doped Hexagonal Boron Nitride (hBN) Films via Co− Sputtering. *Crystals* **2022**, *12*, 777. [CrossRef]
96. Li, L.H.; Xing, T.; Chen, Y.; Jones, R. Boron nitride nanosheets for metal protection. *Adv. Mater. Interfaces* **2014**, *1*, 1300132. [CrossRef]
97. Li, L.; Li, L.H.; Chen, Y.; Dai, X.J.; Lamb, P.R.; Cheng, B.M.; Lin, M.Y.; Liu, X. High-quality boron nitride nanoribbons: Unzipping during nanotube synthesis. *Angew. Chem.* **2013**, *125*, 4306–4310. [CrossRef]
98. Kubota, Y.; Watanabe, K.; Tsuda, O.; Taniguchi, T. Deep ultraviolet light-emitting hexagonal boron nitride synthesized at atmospheric pressure. *Science* **2007**, *317*, 932–934. [CrossRef]
99. Wang, S.; Zhang, L.; Xia, Z.; Roy, A.; Chang, D.W.; Baek, J.B.; Dai, L. BCN graphene as efficient metal-free electrocatalyst for the oxygen reduction reaction. *Angew. Chem. Int. Ed.* **2012**, *51*, 4209. [CrossRef]
100. Zheng, Y.; Jiao, Y.; Ge, L.; Jaroniec, M.; Qiao, S.Z. Two-step boron and nitrogen doping in graphene for enhanced synergistic catalysis. *Angew. Chem. Int. Ed.* **2013**, *52*, 3110–3116. [CrossRef]
101. Khan, M.H.; Jamali, S.S.; Lyalin, A.; Molino, P.J.; Jiang, L.; Liu, H.-K.; Taketsugu, T.; Huang, Z. Atomically thin hexagonal boron nitride nanofilm for Cu protection: The importance of film perfection. *Adv. Mater.* **2017**, *29*, 1603937. [CrossRef]
102. Khan, M.H.; Huang, Z.; Xiao, F.; Casillas, G.; Chen, Z.; Molino, P.J.; Liu, H.K. Synthesis of large and few atomic layers of hexagonal boron nitride on melted copper. *Sci. Rep.* **2015**, *5*, 7743. [CrossRef]
103. Zhou, F.; Li, Z.; Shenoy, G.J.; Li, L.; Liu, H. Enhanced room-temperature corrosion of copper in the presence of graphene. *Acs Nano* **2013**, *7*, 6939–6947. [CrossRef]
104. Niaura, G. Surface-enhanced Raman spectroscopic observation of two kinds of adsorbed OH− ions at copper electrode. *Electrochim. Acta* **2000**, *45*, 3507–3519. [CrossRef]
105. Prasai, D.; Tuberquia, J.C.; Harl, R.R.; Jennings, G.K.; Bolotin, K.I. Graphene: Corrosion-inhibiting coating. *ACS Nano* **2012**, *6*, 1102–1108. [CrossRef] [PubMed]
106. Huh, J.-H.; Kim, S.H.; Chu, J.H.; Kim, S.Y.; Kim, J.H.; Kwon, S.-Y. Enhancement of seawater corrosion resistance in copper using acetone-derived graphene coating. *Nanoscale* **2014**, *6*, 4379–4386. [CrossRef] [PubMed]
107. Ren, S.; Cui, M.; Pu, J.; Xue, Q.; Wang, L. Multilayer regulation of atomic boron nitride films to improve oxidation and corrosion resistance of Cu. *ACS Appl. Mater. Interfaces* **2017**, *9*, 27152–27165. [CrossRef]

108. Shen, L.; Zhao, Y.; Wang, Y.; Song, R.; Yao, Q.; Chen, S.; Chai, Y. A long-term corrosion barrier with an insulating boron nitride monolayer. *J. Mater. Chem. A* **2016**, *4*, 5044–5050. [CrossRef]
109. Poulston, S.; Parlett, P.; Stone, P.; Bowker, M. Surface oxidation and reduction of CuO and Cu_2O studied using XPS and XAES. *Surf. Interface Anal. Int. J. Devoted Dev. Appl. Tech. Anal. Surf. Interfaces Thin Film.* **1996**, *24*, 811–820. [CrossRef]
110. Nadeem, A.; Maqsood, M.F.; Raza, M.A.; Ilyas, M.T.; Iqbal, M.J.; Rehman, Z.U. Binder free boron nitride-based coatings deposited on mild steel by chemical vapour deposition: Anti-corrosion performance analysis. *Phys. B Condens. Matter* **2021**, *602*, 412600. [CrossRef]
111. Pakdel, A.; Zhi, C.; Bando, Y.; Golberg, D. Low-dimensional boron nitride nanomaterials. *Mater. Today* **2012**, *15*, 256–265. [CrossRef]
112. Cui, Z.; Oyer, A.J.; Glover, A.J.; Schniepp, H.C.; Adamson, D.H. Large scale thermal exfoliation and functionalization of boron nitride. *Small* **2014**, *10*, 2352–2355. [CrossRef]
113. Posudievsky, O.Y.; Khazieieva, O.A.; Cherepanov, V.V.; Dovbeshko, G.I.; Koshechko, V.G.; Pokhodenko, V.D. Efficient dispersant-free liquid exfoliation down to the graphene-like state of solvent-free mechanochemically delaminated bulk hexagonal boron nitride. *RSC Adv.* **2016**, *6*, 47112–47119. [CrossRef]
114. Li, X.; Hao, X.; Zhao, M.; Wu, Y.; Yang, J.; Tian, Y.; Qian, G. Exfoliation of hexagonal boron nitride by molten hydroxides. *Adv. Mater.* **2013**, *25*, 2200–2204. [CrossRef] [PubMed]
115. Sherif, E.; Park, S.-M. Inhibition of copper corrosion in 3.0% NaCl solution by N-phenyl-1, 4-phenylenediamine. *J. Electrochem. Soc.* **2005**, *152*, B428. [CrossRef]
116. Wu, Y.; He, Y.; Zhou, T.; Chen, C.; Zhong, F.; Xia, Y.; Xie, P.; Zhang, C. Synergistic functionalization of h-BN by mechanical exfoliation and PEI chemical modification for enhancing the corrosion resistance of waterborne epoxy coating. *Prog. Org. Coat.* **2020**, *142*, 105541. [CrossRef]
117. Tang, X.; Wang, H.; Liu, C.; Zhu, X.; Gao, W.; Yin, H. Direct growth of hexagonal boron nitride nanofilms on stainless steel for corrosion protection. *ACS Appl. Nano Mater.* **2021**, *4*, 12024–12033. [CrossRef]
118. Palai, D.; Bhattacharya, M.; Mallick, A.B.; Bera, P.; Sharma, A.K.; Mukhopadhyay, A.K.; Dey, A. Microstructural, thermo-optical, mechanical and tribological behaviours of vacuum heat treated ultra thin SS304 foils. *Mater. Res. Express* **2016**, *3*, 096501. [CrossRef]
119. Chen, Z.-G.; Zou, J.; Liu, G.; Li, F.; Wang, Y.; Wang, L.; Yuan, X.-L.; Sekiguchi, T.; Cheng, H.-M.; Lu, G.Q. Novel boron nitride hollow nanoribbons. *Acs Nano* **2008**, *2*, 2183–2191. [CrossRef]
120. Borowiak-Palen, E.; Pichler, T.; Fuentes, G.G.; Bendjemil, B.; Liu, X.; Graff, A.; Behr, G.; Kalenczuk, R.J.; Knupfer, M.; Fink, J. Infrared response of multiwalled boron nitride nanotubes. *Chem. Commun.* **2003**, *1*, 82–83. [CrossRef]
121. Gao, M.; Meng, J.; Chen, Y.; Ye, S.; Wang, Y.; Ding, C.; Li, Y.; Yin, Z.; Zeng, X.; You, J. Catalyst-free growth of two-dimensional hexagonal boron nitride few-layers on sapphire for deep ultraviolet photodetectors. *J. Mater. Chem. C* **2019**, *7*, 14999–15006. [CrossRef]
122. Chen, T.-A.; Chuu, C.-P.; Tseng, C.-C.; Wen, C.-K.; Wong, H.-S.P.; Pan, S.; Li, R.; Chao, T.-A.; Chueh, W.-C.; Zhang, Y. Wafer-scale single-crystal hexagonal boron nitride monolayers on Cu (111). *Nature* **2020**, *579*, 219–223. [CrossRef]
123. Liu, J.; Kutty, R.G.; Zheng, Q.; Eswariah, V.; Sreejith, S.; Liu, Z. Hexagonal Boron Nitride Nanosheets as High-Performance Binder-Free Fire-Resistant Wood Coatings. 2016. Available online: https://hdl.handle.net/10356/85139 (accessed on 3 December 2023).
124. Geick, R.; Perry, C.; Rupprecht, G. Normal modes in hexagonal boron nitride. *Phys. Rev.* **1966**, *146*, 543. [CrossRef]
125. Du, M.; Wu, Y.; Hao, X. A facile chemical exfoliation method to obtain large size boron nitride nanosheets. *CrystEngComm* **2013**, *15*, 1782–1786. [CrossRef]
126. Mehdi, S.M.Z.; Maqsood, M.F.; Dahshan, A.; Ahmad, S.; Ur Rehman, M.; Lee, N.; Rehman, M.A.; Khan, M.F. Emerging boron nitride nanosheets: A review on synthesis, corrosion resistance coatings, and their impacts on the environment and health. *Rev. Adv. Mater. Sci.* **2024**, *63*, 20240075. [CrossRef]
127. OpenAI. *GPT-3.5*; OpenAI: San Francisco, CA, USA, 2023. Available online: https://chat.openai.com/ (accessed on 18 November 2024).